Transactions on Energy Systems and Engineering Applications

Article

One- and multi-diode PV module models: PSO-based parameter extraction and performance evaluation under conventional and low-concentration photovoltaic conditions

Olfa Bel Hadj Brahim Kechiche[1,*], Mahmoud Hamouda[2] and Aissa Chouder[3]

[1] Higher School of Science and Technology of Hammam Sousse, Laboratory of Energy and Materials (LR11ES34), University of Sousse, Rue Abbassi Lamine, 4011 Hammam Sousse, Tunisia.
[2] National Engineering School of Sousse, LATIS - Laboratory of Advanced Technology and Intelligent Systems, University of Sousse, 4023 Sousse, Tunisia.
[3] Department of Electronics, Laboratory LGE, University Mohamed Boudiaf of M'sila, 28000 M'sila, Algeria.
* Correspondence: belhajbrahimolfa@yahoo.fr

Received: 02 September 2025; Accepted: 30 January 2026; Published: 10 February 2025

Abstract: This study investigates the performance of diode-based photovoltaic (PV) modules models by analyzing their effectiveness in predicting the electric behviour under conventional solar irradiation and low-concentration photovoltaic (LCPV) conditions. The parameters of one-diode (1-DM), two-diode (2-DM), three-diode (3-DM) and four-diode models (4-DM) are first extracted using the particle swarm optimization technique (PSO) and validated through a comparative analysis with experimental measurements carried out on a PV module (ISOFOTON 106 W-12 V) in real-world temperature and irradiation conditions of 27.2°C and 755W/m^2, respectively. The findings reveal that the 4-DM exhibits the minimum deviation from experimental data in predicting key performance metrics such as short-circuit current (I_{sc}), open-circuit voltage (V_{oc}), and maximum output power (P_m). However, this increased accuracy comes at the cost of higher computational complexity in optimizing the 4-DM's parameters. The studies carried out under several low-concentration photovoltaic conditions show clearly the limitation of the 1-DM in terms of predicted (P_m), efficiency, and fill factor (FF). Indeed, the gaps in the obtained values of efficiency and FF with respect to the 4-DM increase with the concentration ratio and reach 0.74% and 0.04, respectively, at 3 suns. The performances obtained with the 2-DM and 3-DM remain stable and close to those of the 4-DM with constant gaps in the obtained values of efficiency and FF, remaining close to 0.1% and 0.01, respectively, regardless of the concentration ratio. The insights gained from this work underscore the significance of selecting an appropriate PV model for LCPV systems, balancing accuracy and computational efficiency.

How to cite this article: Olfa, BEL HADJ BRAHIM KECHICHE; Mahmoud, HAMOUDA; Aissa, CHOUDER. One- and multi-diode PV module models: PSO-based parameter extraction and performance evaluation under conventional and

1. Introduction

The increasing global demand for renewable energy has driven significant advancements in solar photovoltaic (PV) technology, with a particular focus on improving the efficiency and performance of PV systems under various operating conditions. In 2023, solar PV power generation increased by a record 320 TWh, up by 25% from 2022, accounting for 5.4% of total global electricity generation, [1–3]. Among the key areas of research is the modelling of photovoltaic cells, modules and farms, which is essential for understanding their behaviour and optimizing their performance. Accurate modelling of PV modules enables the prediction of their electrical characteristics under different environmental conditions, such as varying irradiation and temperature, which are critical for designing efficient solar energy systems, [4,5]. In this context, diode-based models, including the one-diode (1-DM), two-diode, (2-DM) three-diode (3-DM), and four-diode models (4-DM), have been developed to reproduce the electrical behaviour of solar PV cells and modules. Each of these models offers different levels of complexity and accuracy, making them suitable for different applications and operating conditions, [6, 7].

Concentration photovoltaic (CPV) systems, which use optical devices such as lenses or mirrors to focus sunlight on PV modules, have gained attention for their ability to enhance energy output. CPV systems are typically classified into three categories based on the concentration ratio: low-concentration photovoltaic (LCPV, less than 10x), medium-concentration photovoltaic (MCPV, 10x to 100x), and high-concentration photovoltaic (HCPV, greater than 100x). LCPV systems, in particular, are of interest for commercial applications due to their moderate concentration levels, which can be achieved without the need for complex optical systems. However, the performance of PV modules under concentrated light is influenced by several factors, including increased temperature, recombination effects, and non-ideal behaviors, which become more pronounced under high irradiation. Therefore, understanding the accuracy of different diode-based models under concentrated light is crucial for optimizing LCPV systems, [8–12]. The 1-DM, while simple and widely used, has limitations in accurately capturing the behavior of PV cells under high irradiance, particularly due to its neglect of recombination effects. As a result, more complex models such as the 2-DM, 3-DM and 4-DM have been developed to better represent the physical phenomena occurring in PV cells under concentrated light. These models incorporate additional diodes to account for recombination currents and other non-ideal effects.

Several studies have investigated methods for estimating PV module parameters, particularly for 1-DM and multi-diode models. Some works have employed heuristic optimization algorithms such as Particle Swarm Optimization (PSO), Genetic Algorithms (GA), and Hybrid Metaheuristic Techniques to enhance parameter extraction accuracy, while others have explored analytical and experimental approaches to refine PV model predictions under various environmental conditions, [13–17]. Yadav et al. [13] analyzed key factors influencing the performance of single- and multi-diode PV modules, including fill factor, material properties, and temperature effects. Their study examined how irradiance variations affect efficiency and system output, providing insights into optimizing PV module design. Meng et al. [14] introduced an efficient method for extracting parameters of the 2-DM using only standard test condition (STC) data from manufacturer datasheets. Their approach, combining initial parameter estimation with a mountain-climbing algorithm, demonstrated superior accuracy in modeling I-V characteristics, particularly at the maximum power point. Kullampalayam Murugaiyan et al. [15] and Qais et al. [16] proposed advanced hybrid methods for parameter estimation in 3-DM. Murugaiyan et al. combined a Reinforced Learning-Based Parrot Optimizer (RLPO) with an Adaptive Secant Method (ASM) to enhance search adaptability and

low-concentration photovoltaic conditions. *Transactions on Energy Systems and Engineering Applications*, 7(1): 931, 2026. DOI:10.32397/tesea.vol7.n1.931

convergence speed, while Qais et al. integrated an analytical approach with the Sunflower Optimization Algorithm (SFOA) to refine parameter estimation. Both methods effectively addressed nonlinearities and recombination losses, demonstrating improved accuracy and convergence. Saripalli et al. [17] developed a hybrid optimization technique for parameter extraction in the 4-DM, combining GA and PSO. Their approach improved parameter estimation efficiency, enhancing the accuracy of I-V characteristic modeling.

While these studies developed advanced parameter extraction methods for multi-diode PV models, they did not evaluate their performance under concentrated solar power (CSP) conditions. Similarly, research on PV module behavior under concentration conditions has largely focused on system-level analysis rather than refining diode-based models to improve accuracy. Some studies analyzed the impact of temperature and optical concentration on efficiency, [10–12], but only a few systematically evaluated different PV models under low-concentration photovoltaic (LCPV) conditions, [18–20]. For instance, Kumar et al. provided a comprehensive review of solar parabolic dish collectors, emphasizing their potential for improving concentrated solar thermal systems. However, their work primarily focused on thermal applications rather than electrical modeling of PV modules. Paul [11] analyzed the application of compound parabolic concentrators (CPC) in PV conversion, detailing their ability to enhance energy capture. While this study discussed system-level efficiency improvements, it did not assess the accuracy of diode-based PV models under concentration conditions. Masood et al. [12] reviewed recent advancements in hybrid photovoltaic/thermal (PV/T) systems incorporating CPCs, highlighting their thermal management benefits but lacking a detailed evaluation of different PV models and their parameter estimation strategies. Yadav et al. [21] specifically examined the effects of temperature and concentration on a commercial silicon-based PV module in an LCPV system. While their study provided valuable insights into performance variations, it did not compare different diode-based models to determine their suitability under concentrated light.

In contrast, our study addresses these gaps by conducting a systematic comparative evaluation of 1-DM, 2D-M, 3D-M and 4-DM under different LCPV conditions. Unlike previous works, we focus on parameter optimization using PSO and assess the trade-off between model complexity and accuracy in predicting key performance metrics under varying concentration ratios. This approach provides a deeper understanding of how different PV models respond to concentrated light, contributing to the optimization of LCPV system designs. Models performances are validated and evaluated through a comparison with experimental data of a commercial PV module (ISOFOTON 106 W-12V) and using also different indicators such as the accuracy in estimating the open-circuit voltage, the short-circuit current, the maximum power as well as the efficiency and fill factor.

This paper is structured as follows: Section 2 and presents an overview of PV module modelling approaches, detailing the characteristics and parameter estimation methods of the 1-DM, 2-DM, 3-DM, and 4-DM. Section 3 describes the application of PSO for parameter extraction, including the fitness function and optimization process. Section 4 focuses on the evaluation of the models performance under conventional solar irradiation and low concentration highlighting the limitation and suitability of each model. Finally, Section 5 concludes the study with a summary of key findings and their implications for LCPV system optimization.

2. Overview of PV modules modeling approaches

2.1. One-diode model (1-DM): 5 parameters

The one-diode equivalent circuit depicted in Figure 1a is widely adopted as the standard approach for photovoltaic (PV) modules modeling since it makes a good compromise between simplicity and accuracy, particularly in the context of energy production, [13, 22]. Diode (D_1) emulates the recombination losses in the PN junction. The series resistor (R_s) represents the equivalent ohmic losses due to the flow of current

through the PV cells. The shunt resistor (R_{sh}) Represents leakage currents and junction edge effects. Its impact is typically less significant than (R_s) in a single module but becomes more pronounced in parallel configurations. Considering the equivalent model depicted in Figure 1a, the relationship between the current I supplied by the PV module and the voltage V across its terminals is:

$$I = I_{ph} - I_{d1} - \frac{V + IR_s}{R_{sh}}, \tag{1}$$

I_{ph} is the photocurrent generated by an ideal PV module and depends on the illuminance and temperature conditions. Id_1 is the current through the ideal diode(D_1) determined as:

$$I_{d1} = I_{s1}\left(\exp\left(\frac{q\,(V + IR_s)}{n_1 k_b T N_s} - 1\right)\right), \tag{2}$$

I_{s1} is the diode saturation current, which is mainly dependent on the temperature condition and bandgap energy. $q = 1.6\text{x}10^{-19}C$ is the electron charge. $k_b = 1.380649 \times 10^{-23} JK^{-1}$ is the Boltzmann constant.N_s is the number of PV cells connected in series. n_1 is the ideality factor of D_1, which quantifies the deviation from the ideal diode's behavior. Replacing eq. (2) into eq. (1) yields the commonly used I-V characteristics of a one-diode PV module:

$$I = I_{ph} - I_{s1}\left(\exp\left(\frac{q\,(V + IR_s)}{n_1 k_b T N_s} - 1\right)\right) - \frac{V + IR_s}{R_{sh}}. \tag{3}$$

Considering the above analytical relationship, it is obvious that the 1-DM relies on five intrinsic parameters of the PV module, which are I_{ph}, I_{s1}, R_s, R_{sh} and n_1. In general, the 1-DM is easy to implement, suitable for fast computation and performs well under standard irradiation conditions. However, it suffers from the drawbacks of low accuracy under non-ideal conditions such as high temperature or low irradiance and fails to capture complex losses like surface recombination.

2.2. Two-diode model (2-DM): 7 parameters

The 2-DM depicted in Figure 1b uses an additional diode D_2 to take account of both bulk and recombination losses, which become significant under high irradiance and temperature conditions. Considering this, the relationship between the PV module current I and the voltage across its terminals V becomes [14, 23, 24]:

$$I = I_{ph} - I_{d1} - I_{d2} - \frac{V + IR_s}{R_{sh}}, \tag{4}$$

I_{d2} is the current through D_2 expressed as follows:

$$I_{d2} = I_{s2}\left(\exp\left(\frac{q\,(V + IR_s)}{n_2 k_b T N_s} - 1\right)\right), \tag{5}$$

I_{s2} is the saturation current of the second diode D_2, representing the recombination current due to carrier recombination in the solar cells. n_2 is the ideality factor of D_2. It usually has a value greater than 2, indicating a higher degree of recombination compared to the first diode. Substituting now eq. (2) and eq. (5) into (4) yields the analytical equivalent 2-DM of the PV module:

$$I = I_{ph} - I_{s1}\left(\exp\left(\frac{q(V+IR_s)}{n_1 k_b T N_s} - 1\right)\right) - I_{s2}\left(\exp\left(\frac{q(V+IR_s)}{n_2 k_b T N_s} - 1\right)\right) \underset{-\frac{V+IR_s}{R_{sh}}}{} . \tag{6}$$

As can be concluded from eq. (6), the 2-DM relies on 7 intrinsic parameters i.e. I_{ph}, I_{s1}, I_{s2}, R_s, R_{sh}, n_1 and n_2. The increased number of parameters compared to the 1-DM improves the model's accuracy by accounting for both bulk and surface recombination losses. It is also more suited to variable irradiation and temperature conditions.

2.3. Three-diode model (3-DM): 9 parameters

Figure 1c depicts the equivalent electrical circuit of a 3-DM, where an additional diode D_3 is used as compared to the 2-DM. The objective is to improve the model accuracy by capturing additional current losses due to specific leakage effects. I_{d3} represents the recombination current due to defects, grain boundaries, and other localized imperfections within the photovoltaic cell, which contribute to additional current losses and affect the cell's overall efficiency, particularly under high-stress conditions such as high temperatures or increased irradiance [25–28]. In view of this, the current supplied by the PV module becomes:

$$I = I_{ph} - I_{d1} - I_{d2} - I_{d3} - \frac{V + IR_s}{R_{sh}}. \tag{7}$$

Define I_{s3} the saturation current of D_3 and n_3 its ideality factor. Therefore, we can likewise express the current through D_3:

$$I_{d3} = I_{s3}\left(\exp\left(\frac{q\,(V + IR_s)}{n_3 k_b T N_s} - 1\right)\right). \tag{8}$$

Note that n_3 has typically a value greater than 3, indicating a higher degree of recombination compared to the first and second diodes. Substituting now eq. (2), eq. (5) and eq. (8) into eq. (7) yields the 3-DM of the PV module, typically relying on 9 intrinsic parameters I_{ph}, I_{s1}, I_{s2}, I_{s3}, R_s, R_{sh}, n_1, n_2 and n_3:

$$\begin{aligned} I = I_{ph} - I_{s1}\left(\exp\left(\tfrac{q(V+IR_s)}{n_1 k_b T N_s} - 1\right)\right) - I_{s2}\left(\exp\left(\tfrac{q(V+IR_s)}{n_2 k_b T N_s} - 1\right)\right) \\ - I_{s3}\left(\exp\left(\tfrac{q(V+IR_s)}{n_3 k_b T N_s} - 1\right)\right) - \tfrac{V+IR_s}{R_{sh}} \end{aligned}. \tag{9}$$

This model is able to provide high accuracy in a wide range of conditions due to the inclusion of additional nonlinear effects. However, the high number of parameters increase its complexity and computational cost.

2.4. Four-diode model (4-DM): 11 parameters

Figure 1d depicts the 4-DM of the PV module. The fourth diode takes account of advanced effects like degradation or multi-interface phenomena. This makes the 4-DM more accurate and suitable for highly detailed simulations of PV systems under diverse environmental conditions, [17, 29, 30]. Note that research papers and scientific works on 4-DM are relatively scarce, as the 3-DM is often sufficient for most practical purposes. But the 4-DM has been used in advanced simulations in cases where precision is critical [31]. Using the same analytical development methodology of the previous sections, the current I_{d4} through D_4 and the resulting current I supplied by the PV module are derived as follows:

$$I_{d4} = I_{s4}\left(\exp\left(\frac{q\,(V + IR_s)}{n_4 k_b T N_s} - 1\right)\right), \tag{10}$$

$$\begin{aligned} I = I_{ph} - I_{s1}\left(\exp\left(\tfrac{q(V+IR_s)}{n_1 k_b T N_s} - 1\right)\right) - I_{s2}\left(\exp\left(\tfrac{q(V+IR_s)}{n_2 k_b T N_s} - 1\right)\right) \\ - I_{s3}\left(\exp\left(\tfrac{q(V+IR_s)}{n_3 k_b T N_s} - 1\right)\right) - I_{s4}\left(\exp\left(\tfrac{q(V+IR_s)}{n_4 k_b T N_s} - 1\right)\right) \\ - \tfrac{V+IR_s}{R_{sh}} \end{aligned}, \tag{11}$$

I_{s4} and n_4 are the fourth diode's saturation current and ideality factor, respectively. n_4 typically exceeds 4, indicating a higher degree of recombination compared to the earlier diodes, particularly under stress conditions. The 4-DM requires the identification of 11 intrinsic parameters I_{ph}, I_{s1}, I_{s2}, I_{s3}, I_{s4}, R_s, R_{sh}, n_1, n_2, n_3 and n_4. It was introduced in the research literature in recent years with the aim to provide the highest level of accuracy for predicting the module performance, especially under high levels of temperature and irradiation. However, the high number of parameters increases gradually its complexity. This model is not yet well explored in the research literature, particularly from the point of view of parameter identification and also its behavior under different operating conditions such as low concentration.

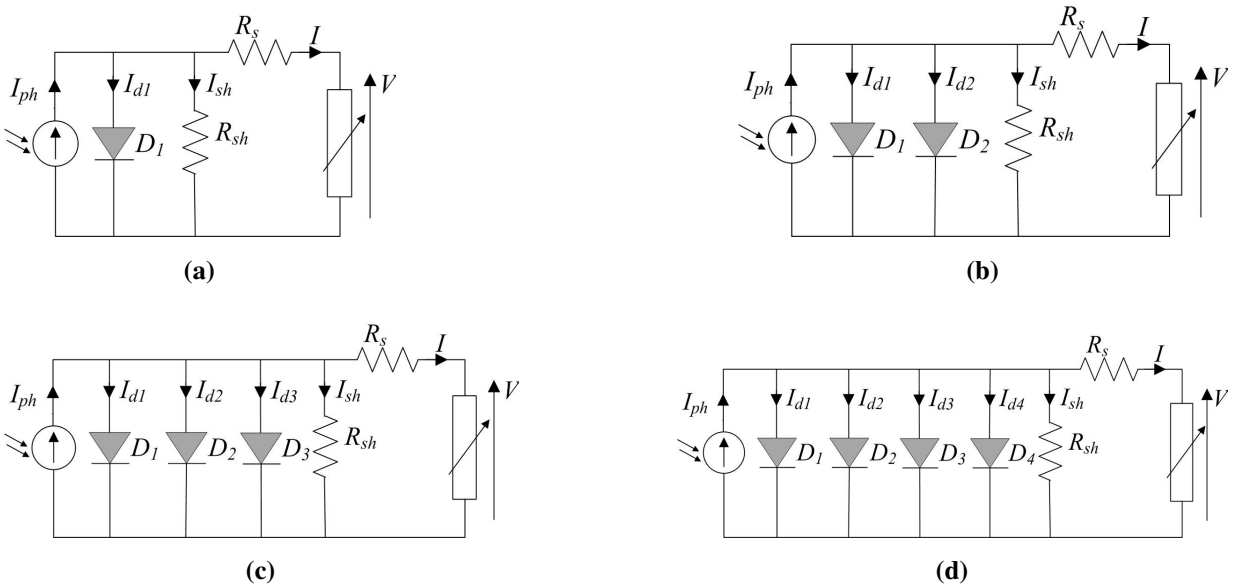

Figure 1. Equivalent electrical circuits of a PV module (a) One-diode model – (b) two-diode model – (c) three-diode model – (d) four-diode model.

3. Optimized Parameters extraction of the four PV models

In this section, we explore the extraction of the four PV module models' key parameters using the data translation method from the International Standard IEC 6089 and Particle Swarm Optimization (PSO) algorithm. This approach is essential for optimizing the performance of PV models under different environmental conditions, including concentration. Through a fine-tuning of each model's parameters, this optimization helps in simulating real-world performance more accurately, particularly under non-ideal conditions such as variations in temperature and irradiance. The results from this optimization process are then used to validate the models, ensuring that the simulations align with actual PV module behavior.

3.1. Translation of the experimental dataset to the reference conditions

In this study, the focus is placed on the "ISOFOTON 106 W-12 V" PV module, serving as a reference for parameters extraction considering the four models under study. The PV module's characteristics as provided by the manufacturer and corresponding to its original state, i.e. zero operating hours are listed in Table 1. An experimental test is carried out to collect a database corresponding to the evolution of the measured PV current and voltage (I_{meas} and V_{meas}) under real environmental condition of temperature (T_{meas}) and irradiation (G_{meas}). Figure 2a and Figure 2b illustrate the I-V and P-V curves (red color) derived from measurements of the ISOFOTON module at $T_{meas} = 27.2°C$ and $G_{meas} = 755W/m^2$. Subsequently,

we translated the obtained data originally collected under non-ideal conditions to STC also referred to as reference conditions i.e. $T_{meas} = 25°C$, $G_{meas} = 1000W/m^2$ air mass value (AM) equal to l.5. Adopting the translation method defined by the International Standard IEC 6089, we first determine the open-circuit voltage and short-circuit current at reference conditions namely $I_{SC,ref}$, $V_{OC,ref}$:

$$I_{SC,ref} = I_{sc,meas}\left(\frac{G_{ref}}{G_{meas}}\right).\left(1 + K_i(T_{ref} - T_{meas})\right), \tag{12}$$

$$V_{OC,ref} = V_{oc,meas} + N_s.n_1\frac{k_b T_{meas}}{q}\ln\left(\frac{G_{ref}}{G_{meas}}\right) + K_v(T_{ref} - T_{meas}) \tag{13}$$

$I_{sc,meas}$, $V_{oc,meas}$ are the short-circuit current and open-circuit voltage obtained from the experimental measurements. Since n_1 is not yet extracted, we will assign the value provided by the technical datasheet to estimate $V_{oc,ref}$. Afterwards, we translate each measured current-voltage pair (I_{meas}, V_{meas}) to its counterpart expected for the reference conditions, namely (I_{ref}, V_{ref}), [32, 33]:

$$I_{ref} = I_{meas} + I_{sc,ref} - I_{sc,meas}, \tag{14}$$

$$V_{ref} = V_{meas} + V_{oc,ref} - V_{oc,meas}. \tag{15}$$

The I-V and P-V curves (blue color) estimated with the translation procedure for the reference conditions are also depicted on the same Figure 2a and Figure 2b (blue color). It can be seen that translated value of the short-circuit current $I_{sc,ref}$ is obtained as 6.7 A and remains very close to manufacturer's specified value, which is equal to 6.54 A. Likewise, the value of the translated open-circuit voltage $V_{oc,ref}$ is equal to 21.38V and remains in the same range as the 21.6 V specified in the datasheet. The small difference falls within an acceptable margin and confirms the reliability of the translation method for estimating the PV module voltage and current in STC.

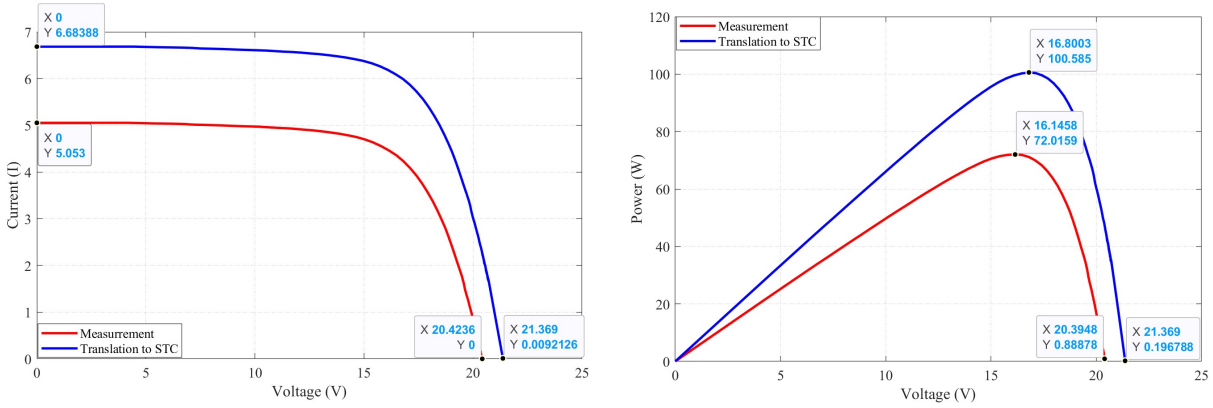

(a) **(b)**

Figure 2. (a) I-V and (b) P-V curves obtained with experimental measurements @ $G_{meas} = 755W/m^2$, $T_{meas} = 27.2\,°C$ (red color) and estimated with the translation procedure for the reference conditions $G_{ref} = 1000W/m^2$, $T_{ref} = 25\,°C$ (blue color).

Table 1. ISOFOTON 106 W-12 V PV module specifications at STC.

Electrical data at STC	
Maximum Power P_m of the PV module (W)	106
Voltage at Maximum Power Point (MPP) V_m (V)	17.4
Current at MPP I_m (A)	6.1
Short-circuit current I_{sc} (A)	6.54
Open-circuit voltage V_{oc} (V)	21.6
Electrical Data at NOCT	
Temperature T_{NOCT} (°C)	47
Thermal Ratings	
K_i (%/°C)	0.06
K_v(%/°C)	-0.36
Material Data	
Cell Type	Mono-crystalline Si
Number of PV cells connected in series (N_s)	36
Number of branches connected in parallel (N_p)	2
Internal parameters	
I_{ph} (A)	6.7043
I_{s1} (A)	1.4058×10^{-7}
n_1	1.1531
R_s (Ω)	0.1516
R_{sh} (Ω)	110
Physical specifications	
Dimensions (mm)	1310/654/39,5
Weight (kg)	11.5
Nominal operating PV cell temperature (°C) @ 800 W m^{-2}, 20 °C, am 1.5, 1 m s^{-1}	47

3.2. Conventional Particle Swarm Optimization (PSO) Based parameters extraction of the four PV models

Particle Swarm Optimization (PSO) is a computational method inspired by the social behavior of birds flocking or fish schooling. In PSO, a population (swarm) of candidate solutions (particles) is iteratively updated based on their individual experiences and the experiences of their neighbors. The algorithm aims to find the optimal solution by adjusting the particles' positions and velocities in the search space according to specific mathematical principles. In this section, the conventional PSO is applied to optimize each diode-model's parameters (1-DM, 2-DM, 3-DM and 4-DM). The optimization process minimizes the error between the I-V curve obtained with the predicted parameters and that obtained with the translated data to the reference conditions [15, 34]. The final objective is to find the parameters set that result in the best match with the real-world performance of the PV module under varying conditions. The rest of this section provides a detailed description of the methodology used to optimize the different models' parameters.

3.2.1. Initialization

The population of particles is first initialized. Each particle represents a possible solution (set of model parameters at reference conditions). Considering the 4-DM, the position vector of each particle is defined as:

$$x_i = [I_{ph,ref,i}, I_{s1,ref,i}, I_{s2,ref,i}, I_{s3,ref,i}, I_{s4,ref}, R_{s,ref,i}, R_{sh,ref,i}, n_{1,ref,i}, n_{2,ref,i}, n_{3,ref,i}, n_{4,ref,i}] \quad . \tag{16}$$

It is worth mentioning that each parameter's boundary should be properly defined to ensure the correct convergence of the algorithm. Table 2 shows the appropriate parameters' boundaries adopted for each diode-model of the PV module "ISOFOTON 106 W-12 V" serving as a case study in this paper.

Table 2. Boundary conditions for PSO algorithm.

Parameter	1-DM	2-DM	3-DM	4-DM
I_{ph} (A)	[5, 8]	[5, 8]	[5, 8]	[5, 8]
I_{s1} (A)	$[10^{-7}, 10^{-4}]$	$[10^{-7}, 10^{-4}]$	$[10^{-7}, 10^{-4}]$	$[10^{-7}, 10^{-4}]$
I_{s2} (A)	–	$[10^{-7}, 10^{-4}]$	$[10^{-10}, 10^{-5}]$	$[10^{-10}, 10^{-5}]$
I_{s3} (A)		–	$[10^{-10}, 10^{-5}]$	$[10^{-10}, 10^{-5}]$
I_{s4} (A)		–		$[10^{-10}, 10^{-5}]$
R_s (Ω)	[0.01, 1]	[0.01, 1]	[0.01, 1]	[0.01, 1]
R_{sh} (Ω)	[0, 400]	[0, 400]	[0, 400]	[0, 400]
n_1	[0, 2]	[0, 2]	[0, 2]	[0, 2]
n_2	–	[0, 5]	[0, 5]	[0, 5]
n_3		–	[0, 5]	[0, 5]
n_4		–		[0, 5]

3.2.2. Fitness Function

The fitness function evaluates how well particle's parameters match the translated data to the reference conditions. This is typically defined as the root mean square error (RMSE) between the estimated I-V curve and its counterpart obtained with the translation procedure to the reference conditions:

$$f(x_i) = \sqrt{\frac{1}{N}\sum_{j=1}^{N}\left(I_{est,j}(x_i) - \mathrm{I}_{ref,j}\right)^2}, \tag{17}$$

$I_{est,j}(x_i)$ is estimated current at point j based on the particle (x_i)'s parameters. $\mathrm{I}_{ref,j}$ is the current at the same point j obtained by the translation procedure and considered as a reference value. N is the number of samples.

3.2.3. Update of velocity and position

The position of each particle (i.e., the model's parameters) is updated based on the particle's previous best position and the global best position found by the swarm as depicted in the flowchart of Figure 3 [35]. The update rules for velocity and position are:

$$\begin{aligned} v_i^{k+1} &= \omega v_i^k + c_1 r_1\left(p_i^k - x_i^k\right) + c_2 r_2\left(g^k - x_i^k\right) \\ x_i^{k+1} &= x_i^k + v_i^{k+1} \end{aligned} \quad , \tag{18}$$

v_i^k is the velocity of particle x_i at iteration k. ω is the inertia weight. c_1 and c_2 are acceleration coefficients. r_1 and r_2 are random numbers between 0 and 1. p_i^k is the personal best position of particle x_i. g^k is the global best position found by the swarm.

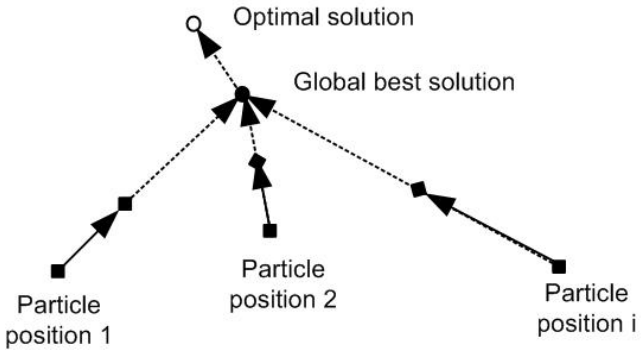

Figure 3. Movement of particles toward the optimal solution.

3.2.4. Convergence and termination

The algorithm iterates until reaching the maximum number of iterations or the defined threshold for the error between the estimated and reference I-V curves. The process is thereafter repeated for each diode-based model to extract the parameters that best fit the translated data. The algorithm was tuned to achieve an optimal balance between accuracy and computational efficiency, with the boundary conditions set as described in Table 2. The obtained optimized parameters at references conditions for each diode-based model are shown in Table 3. One key remark that is worth mentioning is the relatively high value of the estimated resistance in the 1-DM. The impact of this high value on the prediction of power near the maximum power point (MPP) will be examined in a subsequent section.

Table 3. Optimized parameters obtained at reference conditions.

Parameter	1-DM	2-DM	3-DM	4-DM
$I_{ph,ref}$ (A)	6.709	6.709	6.705	6.703
$I_{s1,ref}$ (A)	1×10^{-4}	1×10^{-4}	1×10^{-4}	1×10^{-4}
$I_{s2,ref}$ (A)	–	6.2875×10^{-8}	6.5917×10^{-6}	3.69×10^{-6}
$I_{s3,ref}$ (A)	–	–	3.9115×10^{-7}	9.5738×10^{-7}
$I_{s4,ref}$ (A)	–	–	–	9.748×10^{-7}
$R_{s,ref}$ (Ω)	0.043	0.0431	0.0428	0.070183
$R_{sh,ref}$(Ω)	400	400	400	394.99
$n_{1,ref}$	1.9317	1.9317	1.9377	1.999
$n_{2,ref}$	–	4.4828	4.823	3.819
$n_{3,ref}$	–	–	1.615	1.47
$n_{4,ref}$	–	–	–	4.148

3.2.5. Validation of the optimized parameters' extraction procedure

To validate the effectiveness of the optimized extraction procedure and evaluate its complexity, we compute for each model the RMSE, the Mean Absolute Error (MAE) and the run time. The RMSE and MAE are the errors between the experimental I-V curve translated to the reference conditions and the estimated I-V curve obtained by the diode-based model and considering the optimized parameters extracted at reference conditions. In view of this, the RMSE and MAE are computed as follows:

$$RMSE = \sqrt{\frac{1}{N}\sum_{j=1}^{N}\left(I_{est,j}\left(x_{opt}\right) - \mathrm{I}_{ref,j}\right)^2}, \tag{19}$$

$$MAE = \frac{1}{N}\sum_{j=1}^{n}\left|I_{est,j}\left(x_{opt}\right) - \mathrm{I}_{ref,j}\right|, \tag{20}$$

$I_{est,j}\left(x_{opt}\right)$ is estimated current at point j using the optimized particle $\left(x_{opt}\right)$'s parameters. $\mathrm{I}_{ref,j}$ is the reference current at the same point j obtained by the translation procedure.

Table 4 summarizes the obtained performances with a 64-bit processor running at 3 GHz. In the worst case obtained with the 1-DM, the RMSE and MAE do not exceed 0.304 and 0.2336, respectively, confirming the correct convergence of the PSO algorithm. Moreover, despite the increased complexity of the 4-DM, we confirmed through the outcome of this section that the conventional PSO algorithm is able to successfully optimize the 11 parameters of the 4-DM with a higher accuracy. The correct convergence with this model requires carefully selecting the upper and lower limits of the ideality factor n_4.

When the number of parameters increases from 1-DM (5 parameters) to 4-DM (11 parameters), the computational load increases significantly, with execution time rising from 3.92 seconds to 6.14 seconds. This high cost directly reflects the expansion of the optimization space, which requires broader exploration, greater computational effort per iteration, and more complex convergence dynamics due to the interdependencies between parameters. This additional computational load remains acceptable for offline studies and model identification tasks, where accuracy takes precedence over execution time. However, for real-time or embedded applications, 2-DM and 3-DM configurations offer a more advantageous trade-off between accuracy and computational efficiency. 4-DM remains the best choice for detailed simulations and design optimization, while 1-DM can only be used for quick or low-fidelity estimates.

Practical model selection framework:
The results summarized in Table 4 also serve as a practical decision framework for model selection. The 1-DM is suitable for quick or educational assessments with low computational cost. The 2-DM and 3-DM configurations offer a balanced compromise between accuracy and efficiency, making them appropriate for real-time control or embedded MPPT applications. The 4-DM, while more computationally demanding, provides the highest accuracy and is therefore recommended for offline analysis, detailed simulation, and design optimization tasks.

Table 4. Practical complexity and accuracy indicators for the four diode models.

Model	Parameters	RMSE	MAE	Run Times (s) (PSO, 3 GHz CPU)	Practical recommendation
1-DM	5	0.0304	0.0236	3.92	Fast/low-cost but limited accuracy — not recommended for LCPV high-fidelity studies
2-DM	7	0.0302	0.0234	4.18	Good compromise: moderate cost, good accuracy
3-DM	9	0.02757	0.0228	5.15	Higher fidelity, moderate–high cost
4-DM	11	0.02836	0.0224	6.14	Best accuracy in this study — higher computational cost

3.3. Comparative evaluation of the four models

To validate the effectiveness of the four models, we will conduct a comparative study between the electrical performances predicted by the four models with their optimized parameters and the experimental data measured under real operating conditions. Considering this, we use the following adjustment equations to derive the models' optimized parameters for any other operating condition of temperature T and irradiation G:

$$I_{ph,est} = C\left(I_{ph,ref} + K_i.\left(T - T_{ref}\right)\right), \tag{21}$$

$$n_{\lambda,est} = n_{\lambda,ref}\left(\frac{T}{T_{ref}}\right), \lambda = 1,2,3,4, \tag{22}$$

$$I_{s\lambda,est} = I_{s\lambda,ref}\left(\frac{T}{T_{ref}}\right)^3 \exp\left[\frac{qE_g}{n_\lambda k}\left(\frac{1}{T} - \frac{1}{T_{ref}}\right)\right], \lambda = 1,2,3,4, \tag{23}$$

$$R_{s,est} = R_{s,ref} - \left[\frac{n}{I_{sc,est}}\exp\left(\frac{-V_{oc,est}}{n}\right)\right], \tag{24}$$

$$R_{sh,est} = R_{sh,ref}\left(\frac{G_{ref}}{G}\right), \tag{25}$$

$I_{ph,est}$, $n_{\lambda,est}$, $I_{s\lambda,est}$, $R_{s,est}$ and $R_{sh,est}$ are the optimized models' parameters for a given operating temperature T and irradiation G The subscript λ denotes the diode's number in the model. E_g is the bandgap energy of the semiconductor material used in the construction of the PV cells. It varies with temperature as given by Varshni formula,[8, 36]:

$$E_g(T) = E_g(0) + \frac{\alpha T^2}{T + \beta}, \tag{26}$$

$E_g(0) = 1.1557$, $\alpha = 7.02110^{-4}$ and $\beta = 1108$ are specific empirical constants. $V_{oc,est}$ and $I_{sc,est}$ are the open-circuit voltage and short-circuit current estimated under operating conditions of temperature T and irradiation G:

$$I_{sc,est} = I_{sc,ref}\frac{G}{G_{ref}}\left(1 + K_i(T - T_{ref})\right), \tag{27}$$

$$V_{oc,est} = V_{oc,ref} + N_s.n_1 \frac{k_b T}{q} \ln\left(\frac{G}{G_{ref}}\right) + K_v(T - T_{ref}). \tag{28}$$

By setting $T = T_{meas} = 27.2°C$ and $G = G_{meas} = 755W/m^2$, we can deduce from the transformation Equations (21)-(25) the optimized intrinsic parameters of each model. Afterwards, we implement equations eq. (3), eq. (6), eq. (9) and eq. (11) in Simulink while assigning to the intrinsic parameters of each model their optimized values. A variable resistive load is connected to the equivalent circuits output terminals, making it possible to vary the current produced from 0 (open-circuit) to the short-circuit value. The temperature and irradiation are considered as inputs and are set to $27.2°C$ and $755W/m^2$, respectively. For each operating point selected through the load value, we record the current, voltage and power supplied by the four models.

Figures 4a to 4c illustrates the estimated I-V and P-V curves along with the experimental characteristics, showing how well the four models reproduce the PV module experimental performance under the specified test conditions. The analysis of the obtained performances will focus on the accuracy in predicting three key performance metrics: the short-circuit current I_{sc}, the open-circuit voltage V_{oc} and the maximum power P_m .

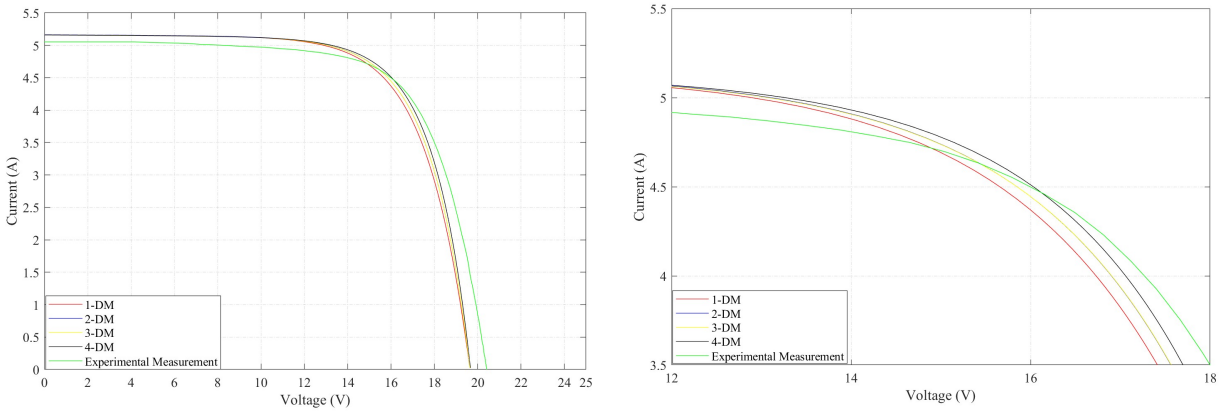

(a) **(b)**

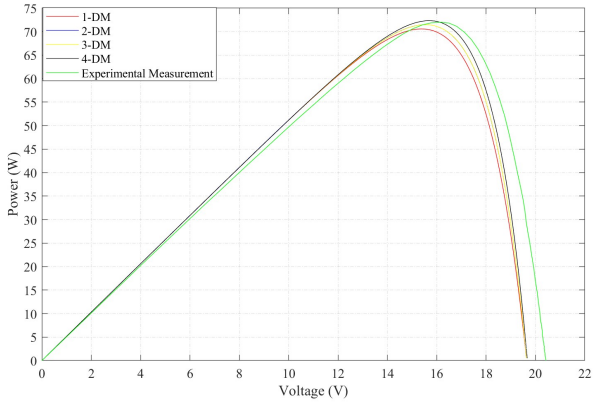

(c)

Figure 4. I-V curves obtained with experimental tests and the prediction models implemented with the PSO optimized parameters (b) zoom in of (a) (c) P-V curves obtained with experimental tests and prediction models.

The effectiveness of the Particle Swarm Optimization (PSO) algorithm in parameters estimation is evident across the four models, as demonstrated by the comparison of predicted results to experimental data reported in Table 5. Indeed, all models provide similar predictions of I_{sc} , with the 4-DM showing the smallest deviation (5.1597 A) from the experimental value of 5.0530 A. This suggests that the conventional PSO algorithm has favorably succeeded in minimizing errors related to the estimation of resistive and photogenerated current parameters. On the other hand, the 4-DM predicts an open-circuit voltage $V_{oc} =$ 19.6629V, remaining the closest to the experimental value of 20.4236 V. Despite these promising results, there were still noticeable discrepancies in the estimation of V_{oc}. This difference could be attributed to the limitations of the translation method used for parameters adjustment. Indeed, the translation method, although useful for simplifying the extraction process, is based on linear approximations, which may not fully account for the non-linear characteristics of photovoltaic systems. As for the maximum power, in all cases, the relative error in its estimate value ε_{pm} remains under 2%. Moreover, the predicted maximum output power by the 4-DM closely matches the experimental value, providing the lowest error of 0.45% and highlighting the superiority of this model. According to this initial validation, the 4-DM model is considered the most complete and accurate model, and therefore, used as the benchmark for the comparative analysis under LCPV.

Table 5. Key performance metrics (I_m, V_m, P_m and η) of the PV module "ISOFOTON 106 W-12 V" obtained with the four prediction models and experimental measurement under T = 27.2 °C and G = 755 W m^{-2}.

Procedure	I_m **(A)**	V_m **(V)**	P_m **(W)**	η **(%)**
1-DM	5.1645	19.6312	70.5845	1.98
2-DM	5.1645	19.6323	71.4784	0.75
3-DM	5.1645	19.6316	71.4701	0.75
4-DM	5.1597	19.6629	72.3434	0.45
Experimental measurement	5.0530	20.4236	72.0159	–

4. Evaluation of the models under low-concentration PV conditions

The purpose of this evaluation is to assess the accuracy and reliability of each model in simulating the performance of the "ISOFOTON 106 W-12 V" photovoltaic module operating under concentrated light. Specifically, we focus on low-concentration photovoltaic (LCPV) conditions. Indeed, low concentration consists in increasing to a certain amount the number of sun rays captured by the PV cells, with the aim of improving the PV module efficiency. One possible solution to provide a low-concentration level of the sunlight is to use a parabolic through concentrator (PLPTC) as described in the subsequent section.

4.1. Brief description of a parabolic concentrator for PV systems

Figure 5 hereafter provides a simplified representation of the PLPTC. It consists of mirror elements mounted on a parabolic structure, together constituting a parabolic reflector. The latter focuses on the incident sunlight onto the PV module surface causing an amplification of the received light by the PV cells. The parabolic reflector may also be mounted on a tracking mechanism (not shown in Fig 5), enabling the system to operate with an optimal sun alignment. Authors showed in [8] that the PLPTC is capable of providing a substantial boosting of the solar irradiation reaching the PV cells, enabling them to operate

with a higher efficiency. Considering the geometrical form of the PLPTC, its focal length F, rim angle ϕ_{rim} and the acceptance angle θ_c are determined as follows:

$$F = \frac{W^2}{16D}, \tag{29}$$

$$\cos(\phi_{rim}) = \left(\frac{2F}{\sqrt{(0.5W)^2 + (D-F)^2}} \right) - 1, \tag{30}$$

$$\sin(\theta_c) = \frac{R_{\min}(1 + \cos(\phi_{rim}))}{2F}, \tag{31}$$

W and D are the width and depth of the parabolic reflector, respectively. $R_{\min}$ is the half width of the PV module. Considering this, the aperture effective area (AE) and concentration level (C) are determined as follows, [21]:

$$AE = W - 2R_{\min}\cos(\phi_{rim} - \theta_c)\, L, \tag{32}$$

$$C_r = 180 \left(\frac{\sin(\phi_{rim}) - \sin(\theta_c)\cos(\phi_{rim} - \theta_c)}{\pi(\phi_{rim} + 90 - \theta_c)\sin(\theta_c)} \right), \tag{33}$$

L is the length of the parabolic reflector. A detailed explanation of the theoretical concept on which the concentrator's operation principle is based could be found in reference, [21].

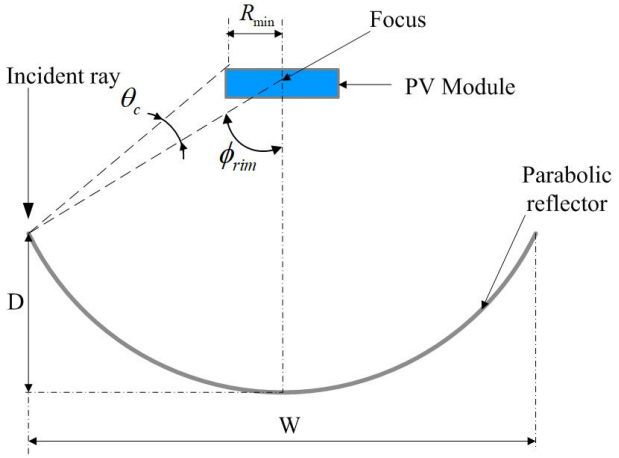

Figure 5. Simplified representation of a parabolic concentrator for PV systems adopted from [21] with some modifications.

4.2. Performance evaluation under different low- concentration conditions

The four models are now simulated with their optimized parameters under different low-concentration conditions. In this section, the concentration factor C is defined as the ratio between the irradiation received by the PV cell (G) and the reference irradiation G_{ref} at STC:

$$C = \frac{G}{G_{ref}}. \tag{34}$$

In order to avoid further complicating this study without missing the originality of the analysis, it will be assumed that the PV module is equipped with a cooling system so that its operating temperature is

maintained constant at 35 °C regardless of the concentration levels, [37,38]. This assumption is introduced in order to dissociate the effect of irradiance from thermal effects and to make a consistent comparison of the models studied under similar temperature conditions. The objective of this study is to evaluate the sensitivity of the single-diode and multi-diode models studied to variations in irradiance, without incorporating coupled temperature fluctuations that could mask differences in model performance. However, this assumption does not reflect the actual operating conditions of concentrated photovoltaic (CPV) systems. In practical applications, if cell cooling is not ideal, an increase in irradiance concentration generally leads to a significant increase in temperature. This increase typically results in a drop in open-circuit voltage (V_{oc}), a decrease in conversion efficiency, and potential discrepancies in model accuracy, particularly for models involving temperature-dependent parameters.

Figures 6a to 6d illustrate the I-V and P-V curves estimated using the four models under different concentration levels ranging from 1 sun ($C = 1$) to 3 suns ($C = 3$). The obtained plots highlight the impact of increasing irradiance on the output current and power, as well as the discrepancies between the different diode models, particularly near the maximum power point (MPP). Additionally, by inspecting the plots in Figures 7a and 7b, showing the maximum power estimated by the four models under different concentration ratios, we can observe that the gap between the 1-DM and 4-DM becomes more important with the increase of C. The difference is about 3 W under 1 sun rising to approximately 30 W when C is set to 3 suns. As for the 2-DM and 3-DM, the gap with respect to the 4-DM remains always around 2 W over the entire C operating range. In our opinion, the important gap observed in the estimation results provided by the 1-DM is due to the lack of precision in estimating the recombination losses in the PN junction, modeled by the diode D_1. Consequently, the value of R_s is adjusted by the optimization algorithm to compensate for the inaccurate estimation of losses due to the recombination current. This will inherently lead to an over-estimation of the series resistance R_s, resulting in an over-prediction of the ohmic losses near the region of MPP.

This behavior demonstrates that the PSO algorithm compensates for the structural constraints of 1-DM by artificially increasing R_s, as the model does not allow for the physical separation of restructuring and resistant losses. This reveals a fundamental weakness of classical models: while optimization can reduce adjustment errors, it cannot substitute for missing physical mechanisms, leading to parameter distortion rather than a true representation of the loss phenomenon. Further quantitative analysis of the diode-based models is carried out on the basis of two additional performance indicators:

The fill factor (FF) indicates the quality of the solar PV module. It is defined as the ratio between the maximum power supplied by the module (P_m) and the product of the short-circuit current by the open-circuit output voltage.

$$FF = \frac{P_m}{I_{sc} \cdot V_{oc}}. \tag{35}$$

The PV module efficiency (η) defined as the ratio of the maximum output power to the input power:

$$\eta = \frac{P_m}{CP_{in}} = \frac{I_{sc} \cdot V_{oc} \cdot FF}{CP_{in}}, \tag{36}$$

P_{in} is the incident power under 1 sun and depends on the module surface (S):

$$P_{in} = S\ G_{ref}. \tag{37}$$

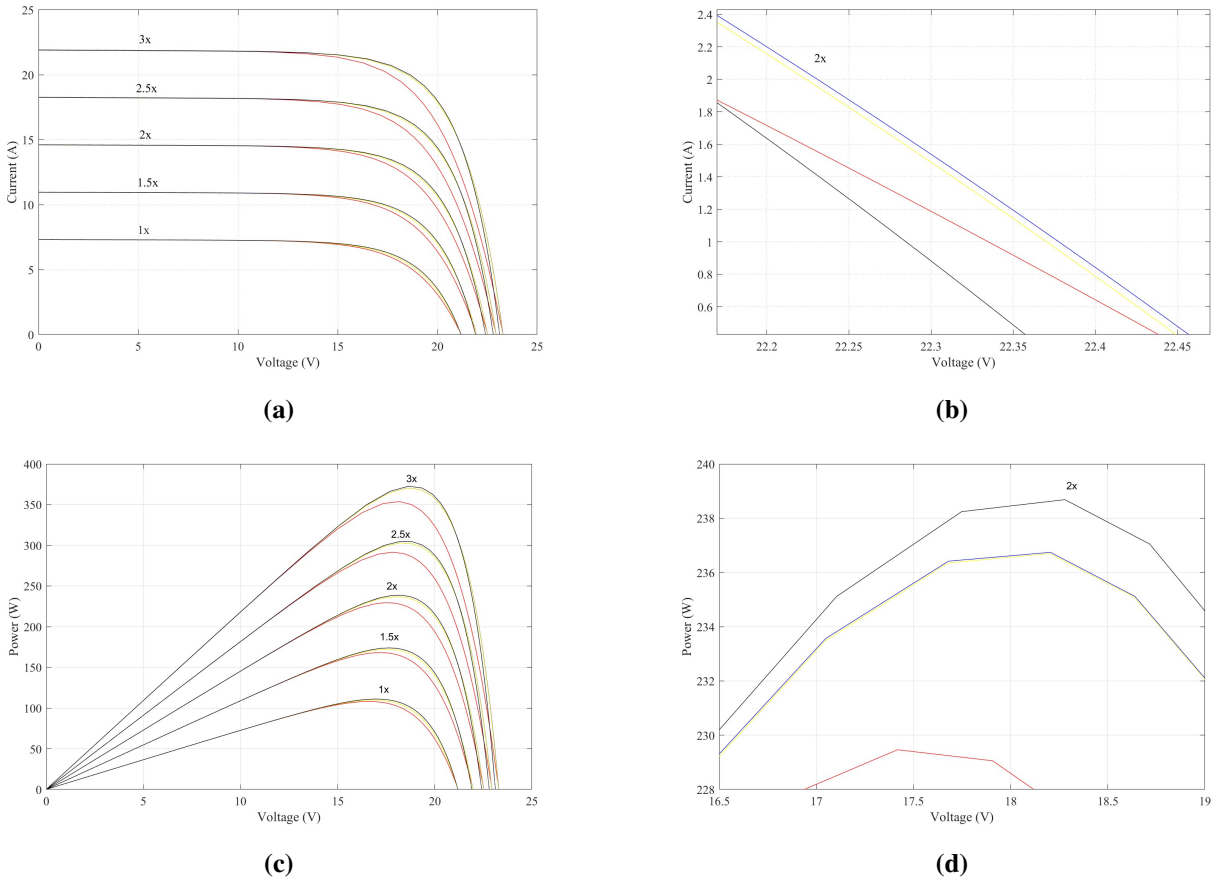

(a) **(b)**

(c) **(d)**

Figure 6. (a) I-V and (b) P-V curves obtained with four models under different concentration ratios and an operating temperature of 35 °C, (c) zoom in of "a" near the open-circuit voltage for C equal to 2 suns, and (d) zoom in of "b" near the maximum power region for C equal to 2 suns.

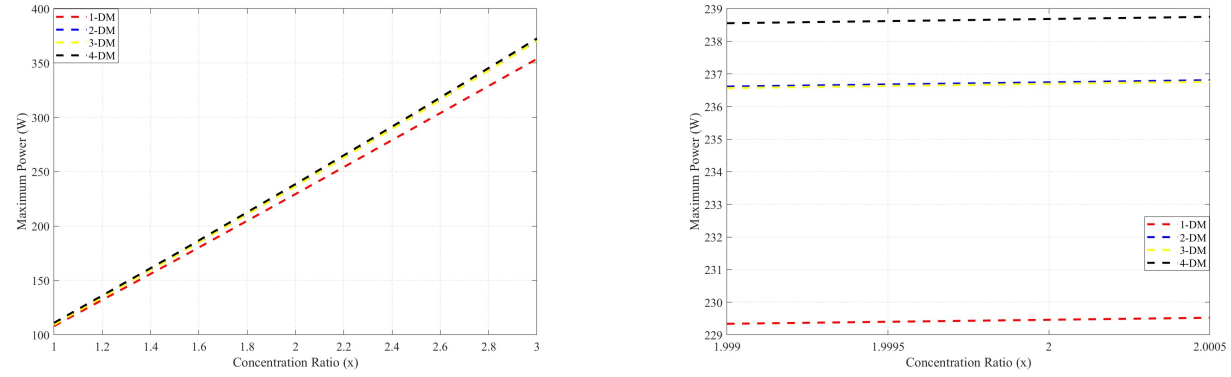

(a) **(b)**

Figure 7. (a) Variation of the maximum power estimated by the four model for different values of C and an operating temperature of 35 °C, (b) zoom in of "a".

Figure 8 illustrates the variation of the Fill Factor versus the concentration ratio obtained with the four models. The results highlight a consistent improvement in the FF as the number of diodes increases, with the four-diode model demonstrating the highest values across all concentration levels. The largest gap with

respect to the 4-DM is obtained with the 1-DM. The difference is about 0.02 under 1 sun and gradually increases with C to reach 0.04 under 3 suns. Moreover, as opposed to the remaining 3 models, the FF estimated by the 1-DM starts to decrease when C reaches 15 suns. On the other hand, 2-DM and 3-DM provide approximately the same performance, while maintaining a constant gap not exceeding 0.01 over the whole operating range of C.

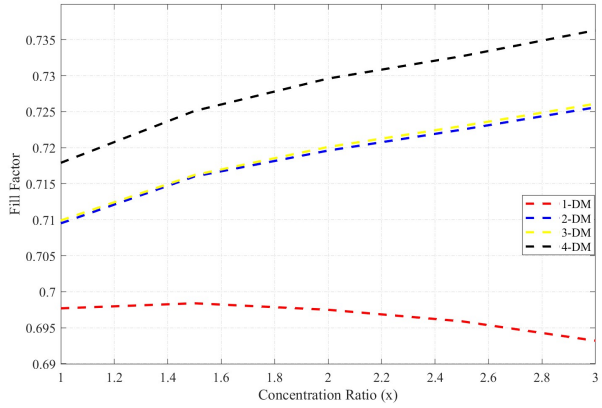

Figure 8. Fill factor of the diode models versus the concentration ratio.

Figure 9 depicts the variation of the efficiency as a function of the concentration ratio C. All models show a positive correlation of the efficiency with the concentration, while the 4-DM provides the best ratio of 14.5% at 3 suns. Similar to the FF trends; the 2-DM and 3-DM provide almost the same efficiency regardless of the concentration ratio. The gap with respect to the 4-DM is practically constant and remains in the region of 0.1%. As for the 1-DM, the gap with respect to the 4-DM is more important. Moreover, it increases with the concentration starting with an error of 0.35% at 1 sun to reach 0.74% at 3 suns.

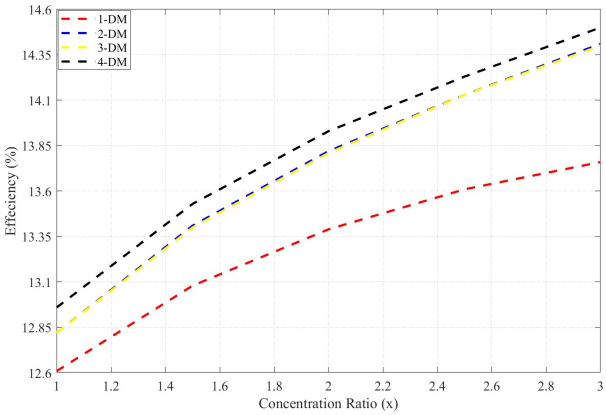

Figure 9. Efficiency trends of the diode models versus the concentration ratio.

In view of the above analysis of the obtained performance indicators, we can confirm that the 2-DM, 3-DM and 4-DM provide stable performances and show the same trends as a function of concentration ratio C. The 2-DM and 3-DM provide approximately similar performance with a low error compared to the 4-DM. The 1-DM provides large errors in all cases with a gradual increase versus the concentration ratio. This is mainly due to the 1-DM' error in predicting the maximum power, which stems from an inadequate balance between different losses mechanisms (recombination losses vs. ohmic losses).

5. Conclusions

This paper investigated the performance of four diode-based PV models using parameters optimized with the conventional Particle Swarm Optimization (PSO) algorithm. Although PSO is widely applied for parameter extraction in PV modeling, this study demonstrates its strong capability in handling complex models such as the 3-DM and 4-DM, which require the estimation of 9 and 11 parameters, respectively. The study also highlights the importance of properly defining the search range of the fourth diode ideality factor to ensure reliable convergence of PSO for the 4-DM.

The accuracy of each model was validated against experimental measurements acquired under real operating conditions. Computational analysis showed that higher-order models increase runtime but also improve accuracy. As a result, the 1-DM model is suitable for quick, low-fidelity estimates, the 2-DM and 3-DM models offer a balanced compromise between accuracy and complexity for real-time use, and the 4-DM model is best suited for offline design and high-precision simulation. These results illustrate the behavior of the model under low-concentration radiation and provide practical guidance for selecting the most appropriate photovoltaic model in research and engineering applications.

Although the low-concentration evaluation was performed at a fixed temperature to isolate the effects of irradiance, in actual CPV systems, cell temperature is expected to increase with concentration if they are not actively cooled. This temperature increase could reduce open-circuit voltage and conversion efficiency, and influence the accuracy of the model, especially for temperature-sensitive parameters. Future studies should therefore consider the combined effects of irradiance and temperature to assess the robustness of the model under realistic thermal conditions.

Funding: This research received no external funding.

Author contributions: Olfa Bel Hadj Brahim: Conceptualization, Methodology, Investigation, Writing – original draft. Mahmoud Hamouda: Supervision, Validation, Writing – review – editing. Aissa Chouder: Supervision, Validation.

Disclosure statement: The authors declare no conflicts of interest.

References

[1] Gaëtan Masson, Melodie de l'Epine, and Izumi Kaizuka. Technology Collaboration Programme by International Energy Agency Photovoltaic Power Systems Programme PVPS Task 1 Strategic PV Analysis and Outreach. Technical report, IEA Photovoltaic Power Systems Programme (PVPS), 2024. Accessed: 2026-02-02.

[2] F. Bariloche. SCIENCE AND ACADEMIA AEE-Institute for Sustainable Technologies (AEE-INTEC) Council on Energy, Environment and Water (CEEW). Technical report, Council on Energy, Environment and Water (CEEW), 2024. Accessed: 2026-02-02.

[3] Olorunshogo Benjamin Ogundipe, Azubuike Chukwudi Okwandu, and Sanni Ayinde Abdulwaheed. Recent advances in solar photovoltaic technologies: Efficiency, materials, and applications. *GSC Advanced Research and Reviews*, 20(1):159–175, July 2024.

[4] Eduardo Manuel Godinho Rodrigues, Radu Godina, Mousa Marzband, and Edris Pouresmaeil. Simulation and Comparison of Mathematical Models of PV Cells with Growing Levels of Complexity. *Energies*, 11(11):2902, October 2018.

[5] Mohammed Aidoud, Chams-Eddine Feraga, Mohcene Bechouat, Moussa Sedraoui, and Sami Kahla. Development of photovoltaic cell models using fundamental modeling approaches. *Energy Procedia*, 162:263–274, April 2019.

[6] Dalia Yousri, Dalia Allam, M.B. Eteiba, and Ponnuthurai Nagaratnam Suganthan. Static and dynamic photovoltaic models' parameters identification using Chaotic Heterogeneous Comprehensive Learning Particle Swarm Optimizer variants. *Energy Conversion and Management*, 182:546–563, February 2019.

[7] Manish Kumar Singla, Mohammad Aljaidi, Jyoti Gupta, Murodbek Safaraliev, Ramesh Kumar, Ziad M Ali, Mohammed H Alsharif, and Mun-Kyeom Kim. Optimizing solar cell models: a multi-objective parameter estimation algorithm for improved photovoltaic system performance. *Physica Scripta*, 100(1):016006, December 2024.

[8] Olfa Bel Hadj Brahim Kechiche and Marwa Hamza. Enhancement of a commercial PV module performance under Low Concentrated Photovoltaic (LCPV) conditions: A numerical study. *Renewable Energy Focus*, 41:258–267, June 2022.

[9] Olfa Bel Hadj Brahim Kechiche and Habib Sammouda. *Concentrator Photovoltaic System (CPV): Maximum Power Point Techniques (MPPT) Design and Performance*. IntechOpen, October 2022.

[10] Kolli Harish Kumar, Ahmed M. Daabo, Malay K. Karmakar, and Harish Hirani. Solar parabolic dish collector for concentrated solar thermal systems: a review and recommendations. *Environmental Science and Pollution Research*, 29(22):32335–32367, February 2022.

[11] Damasen Ikwaba Paul. Application of compound parabolic concentrators to solar photovoltaic conversion: A comprehensive review. *International Journal of Energy Research*, 43(9):4003–4050, April 2019.

[12] Faisal Masood, Nursyarizal Bin Mohd Nor, Perumal Nallagownden, Irraivan Elamvazuthi, Rahman Saidur, Mohammad Azad Alam, Javed Akhter, Mohammad Yusuf, Mubbashar Mehmood, and Mujahid Ali. A Review of Recent Developments and Applications of Compound Parabolic Concentrator-Based Hybrid Solar Photovoltaic/Thermal Collectors. *Sustainability*, 14(9):5529, May 2022.

[13] Dilip Yadav, Nidhi Singh, Vikas Singh Bhadoria, Vasiliki Vita, Georgios Fotis, Eleftherios G. Tsampasis, and Theodoros I. Maris. Analysis of the Factors Influencing the Performance of Single- and Multi-Diode PV Solar Modules. *IEEE Access*, 11:95507–95525, 2023.

[14] Zhuo Meng, Yiman Zhao, Shiqing Tang, and Yize Sun. An efficient datasheet-based parameters extraction method for two-diode photovoltaic cell and cells model. *Renewable Energy*, 153:1174–1182, June 2020.

[15] Nandhini Kullampalayam Murugaiyan, Kumar Chandrasekaran, Magdalin Mary Devapitchai, and Tomonobu Senjyu. Parameter Estimation of Three-Diode Photovoltaic Model Using Reinforced Learning-Based Parrot Optimizer with an Adaptive Secant Method. *Sustainability*, 16(23):10603, December 2024.

[16] Mohammed H. Qais, Hany M. Hasanien, and Saad Alghuwainem. Identification of electrical parameters for three-diode photovoltaic model using analytical and sunflower optimization algorithm. *Applied Energy*, 250:109–117, September 2019.

[17] Bhanu Prakash Saripalli, Bharati Gamgula, Revathi Ravilisetty, Prashant Kumar, Gagan Singh, and Sonika Singh. Advanced parameter extraction optimization technique for the four-diode model approach. *e-Prime - Advances in Electrical Engineering, Electronics and Energy*, 10:100861, December 2024.

[18] Wafa Ben Youssef, Taher Maatallah, Christophe Menezo, and Sassi Ben Nasrallah. Modeling and optimization of a solar system based on concentrating photovoltaic/thermal collector. *Solar Energy*, 170:301–313, August 2018.

[19] Lifeng Li, Bo Wang, Johannes Pottas, and Wojciech Lipiński. Design of a compound parabolic concentrator for a multi-source high-flux solar simulator. *Solar Energy*, 183:805–811, May 2019.

[20] Mohamed Elashmawy. Improving the performance of a parabolic concentrator solar tracking-tubular solar still (PCST-TSS) using gravel as a sensible heat storage material. *Desalination*, 473:114182, January 2020.

[21] Pankaj Yadav, Brijesh Tripathi, Makarand Lokhande, and Manoj Kumar. Effect of temperature and concentration on commercial silicon module based low-concentration photovoltaic system. *Journal of Renewable and Sustainable Energy*, 5(1), January 2013.

[22] Bhanu Prakash Saripalli, Gagan Singh, and Sonika Singh. Cell Modelling and Analysis of Five-Parameter Three Diode model of Photovoltaic Module. In *2021 IEEE 4th International Conference on Computing, Power and Communication Technologies (GUCON)*, page 1–7. IEEE, September 2021.

[23] Habbati Bellia Assia and Moulay Benine Fatima. Detailed modeling of two diode photovoltaic module using MATLAB simulik. *International Journal of Power Electronics and Drive Systems (IJPEDS)*, 10(3):1603, September 2019.

[24] Saripalli Bhanu Prakash, Gagan Singh, and Sonika Singh. Modeling and Performance Analysis of Simplified Two-Diode Model of Photovoltaic Cells. *Frontiers in Physics*, 9, October 2021.

[25] KN Ukoima and OA Ekwe. Three-diode model and simulation of photovoltaic (PV) cells. *Umudike J Eng Technol (UJET)*, pages 108–116, 2019.

[26] Vandana Khanna, B.K. Das, Dinesh Bisht, Vandana, and P.K. Singh. A three diode model for industrial solar cells and estimation of solar cell parameters using PSO algorithm. *Renewable Energy*, 78:105–113, June 2015.

[27] Kensuke Nishioka, Nobuhiro Sakitani, Yukiharu Uraoka, and Takashi Fuyuki. Analysis of multicrystalline silicon solar cells by modified 3-diode equivalent circuit model taking leakage current through periphery into consideration. *Solar Energy Materials and Solar Cells*, 91(13):1222–1227, August 2007.

[28] Hazem Hassan Ellithy, Adel M. Taha, Hany M. Hasanien, Mahmoud A. Attia, Adel El-Shahat, and Shady H. E. Abdel Aleem. Estimation of Parameters of Triple Diode Photovoltaic Models Using Hybrid Particle Swarm and Grey Wolf Optimization. *Sustainability*, 14(15):9046, July 2022.

[29] Beant Singh, Manish Kumar Singla, and Parag Nijhawan. Parameter estimation of four diode solar photovoltaic cell using hybrid algorithm. *Energy Sources, Part A: Recovery, Utilization, and Environmental Effects*, 44(2):4597–4613, May 2022.

[30] Ali M. Jasim, Baraa M. Albaker, and Hussein Jumma Jabir. Modeling and Simulation of Simplified Quadruple Diode Solar PV Module Under Influence of Environmental Conditions and Parasitic Resistance. *TEM Journal*, page 757–770, February 2024.

[31] Manish Kumar Singla, Jyoti Gupta, Mohammed H. Alsharif, Mun-Kyeom Kim, Mohammad Aljaidi, and Murodbek Safaraliev. A robust multi-objective optimization algorithm for accurate parameter estimation for solar cell models. *Soft Computing*, 28(19):11265–11277, July 2024.

[32] Baojie Li, Demba Diallo, Anne Migan-Dubois, and Claude Delpha. Performance evaluation of IEC 60891:2021 procedures for correcting I–V curves of photovoltaic modules under healthy and faulty conditions. *Progress in Photovoltaics: Research and Applications*, 31(5):474–493, November 2022.

[33] Michel Piliougine, Paula Sánchez-Friera, and Giovanni Spagnuolo. Comparative of IEC 60891 and Other Procedures for Temperature and Irradiance Corrections to Measured I–V Characteristics of Photovoltaic Devices. *Energies*, 17(3):566, January 2024.

[34] Hugo Nunes, Jose Pombo, Joao Fermeiro, Silvio Mariano, and Maria do Rosario Calado. Particle Swarm Optimization for photovoltaic model identification. In *2017 International Young Engineers Forum (YEF-ECE)*, page 53–58. IEEE, May 2017.

[35] Rongjie Wang. Parameter Identification of Photovoltaic Cell Model Based on Enhanced Particle Swarm Optimization. *Sustainability*, 13(2):840, January 2021.

[36] K. P. O'Donnell and X. Chen. Temperature dependence of semiconductor band gaps. *Applied Physics Letters*, 58(25):2924–2926, June 1991.

[37] Carlo Renno and Fabio Petito. Design and modeling of a concentrating photovoltaic thermal (CPV/T) system for a domestic application. *Energy and Buildings*, 62:392–402, July 2013.

[38] Joseph Appelbaum and Tamir Maor. Dependence of PV Module Temperature on Incident Time-Dependent Solar Spectrum. *Applied Sciences*, 10(3):914, January 2020.